The Min system disassembles FtsZ foci and inhibits polar peptidoglycan remodeling in *Bacillus subtilis*

Yuanchen Yu[1], Jinsheng Zhou[1], Felix Dempwollf[2], Joshua D. Baker[1], Daniel B. Kearns[2,3], Stephen C. Jacobson[1,3]

[1]Department of Chemistry, Indiana University Bloomington IN USA

[2]Department of Biology, Indiana University Bloomington IN USA

[3]Co-corresponding authors

dbkearns@indiana.edu

jacobson@indiana.edu

Running title: Microfluidic analysis of FtsZ positioning

Keywords: FtsZ, MinD, microfluidics, growth, cell division, peptidoglycan

ABSTRACT

A microfluidic system coupled with fluorescence microscopy is a powerful approach for quantitative analysis of bacterial growth. Here, we measure parameters of growth and dynamic localization of the cell division initiation protein FtsZ in *Bacillus subtilis*. Consistent with previous reports, we find that after division FtsZ rings remain at the cell pole, and FtsZ ring disassembly coincides with rapid Z-ring accumulation at the midcell. In cells mutated for *minD*, however, the polar FtsZ rings persist indefinitely, suggesting that the primary function of the Min system is in Z-ring disassembly. The inability to recycle FtsZ monomers in the *minD* mutant results in maintenance of multiple Z-rings simultaneously, that are restricted by competition for newly synthesized FtsZ. Whereas the parameters of FtsZ dynamics change in the *minD* mutant, the overall cell cycle remains the same, albeit with elongated cells necessary to accumulate a threshold concentration of FtsZ for promoting medial division. Finally, the *minD* mutant characteristically produces minicells composed of polar peptidoglycan shown to be inert for remodeling in the wild type. Polar peptidoglycan, however, loses its inert character in the *minD* mutant suggesting that not only is the Min system important for recycling FtsZ but also may have a secondary role in the regulation of peptidoglycan remodeling.

IMPORTANCE

Many bacteria grow and divide by binary fission in which a mothercell divides into two identical daughter cells. To produce two equally sized daughters, the division machinery, guided by FtsZ, must dynamically localize to the midcell each cell cycle. Here, we quantitatively analyze FtsZ dynamics during growth and find that the Min system of *Bacillus subtilis* is essential to disassemble FtsZ rings after division. Moreover, a failure to efficiently recycle FtsZ results in an increase in cell size. Finally, we show that the Min system has an additional role in inhibiting cell wall turnover and contributes to the “inert” property of cell walls at the poles.

INTRODUCTION

Bacillus subtilis is a gram-positive rod-shaped bacterium that grows and divides by a process called binary fission, in which cells increase in mass and divide into two daughters of roughly equal size. During growth, the cell elongates by inserting new peptidoglycan into the lateral cell wall (1). As biomass increases, replication of the chromosome is initiated, and the chromosomes segregate such that the bulk of the nucleoids become evenly spaced within the cytoplasm (2). Cell division is initiated near the geometric midpoint of the cell where peptidoglycan synthesis is reoriented inward towards the cytoplasm to build a septum and complete cytokinesis (3). Medial positioning of cell division ensures that the septum forms between the two nucleoids, guaranteeing each daughter receives one copy of the chromosome. Although the mechanisms governing growth and cell division-site selection are complex, one of the first factors involved in cell division is the protein, FtsZ.

FtsZ is a homolog of eukaryotic tubulin and exists in two different states in the cytoplasm, either as soluble monomers or in long filamentous polymers called protofilaments (4, 5). The two states rapidly interchange as protofilaments dynamically travel by a process called treadmilling in which FtsZ monomers are added to one end and lost from the other (4, 6-11). Treadmilling protofilaments form on the cytoplasmic facing of the membrane and coalesce into a bright focus called the Z-ring at the nascent site of cell division (12-14). Once mature, the Z-ring recruits a transmembrane complex of proteins known as the divisome that synthesizes peptidoglycan on the outside of the cell (15, 16). The Z-ring constricts, either on its own or aided by divisome-directed peptidoglycan synthesis, until the septum is complete, resulting in cytokinesis (17, 18). Thus, FtsZ is both dynamic and seemingly static when concentrated at the site of cell division, and one of the first recognized factors in controlling FtsZ dynamics and localization is the Min system.

The Min system was first discovered in *E. coli* in the form of a mutant that produced minicells at high frequency (19). Minicells are small, metabolically active, spherical bodies that

lack DNA and arise when cell division occurs, not at the midcell, but rather near one cell pole. Polar division was attributed to a mislocalization of FtsZ rings and the recruitment of the same machinery that would ordinarily promote medial septation (20). The mutation responsible for minicell formation was mapped to a genetic locus encoding the membrane-associated ATPase MinD and the FtsZ-inhibitor MinC (21, 22). MinD is anchored to the membrane by an amphipathic helix, and MinD recruits and activates MinC by direct interaction (23-30). MinC binds to the C-terminus of FtsZ and destabilizes the FtsZ ring (31-35). In *E. c*oli, the activity of the MinCD complex is dynamically restricted to the polar region by oscillation in which MinCD polar polymerization is antagonized by MinE-mediated depolymerization (36-40). In *B. subtilis* however, the activity of the MinCD complex is statically restricted to membranes with high curvature by MinJ/DivIVA, such that the entire 4-protein complex assembles at the invaginating nascent division plane and remains at the cell poles after division (41-46).

Here, we use fluorescence microscopy and microfluidics to quantitatively measure parameters of *B. subtilis* FtsZ dynamics and cell division under the condition of chemostatic growth for extended periods of time (47-52). The automated poly(dimethylsiloxane) microfluidic system comprises a pneumatically actuated channel array of 600 channels having widths from 1.0 to 1.6 μm and heights of 1.0 μm to actively trap bacteria cells (52). Integrated pumps and valves perform on-chip fluid and cell manipulations that provide dynamic control of cell loading and nutrient flow, and the channel array confines bacterial growth to a single dimension, facilitating high-resolution, time-lapse imaging and tracking of individual cells over multiple generations. In wild type cells, we find that Z-rings persist for a period greater than one cell cycle because Z-rings transiently remain at the cell poles following septum completion. We further show find that the primary function of the Min system is Z-ring disassembly such that in the absence of Min, Z-rings persist longer than the duration of the experiment. Indefinite Z-ring persistence results in cells with multiple Z-rings per compartment, and Z-ring must directly compete for newly synthesized FtsZ monomers. Moreover, we show that *min* mutant cells are

101 elongated because of a failure to recycle monomers, and competition between multiple Z-rings
102 necessitates a larger FtsZ pool. Finally, we provide evidence that the *B. subtilis* Min system
103 also inhibits cell wall turnover, particularly at the poles of the cell, and is a contributing factor to
104 reports of inter-polar peptidoglycan.

MATERIALS AND METHODS:

Strains and growth conditions: *B. subtilis* strains were grown in lysogeny broth (LB) (10 g tryptone, 5 g yeast extract, 10 g NaCl per L) or on LB plates fortified with 1.5% Bacto agar at 37˚C.

Microfluidic system: The microfluidic device was fabricated through a combination of electron-beam lithography, contact photolithography, and polymer casting (52). Briefly, the microfluidic device is comprised of fluid and control layers both cast in poly(dimethylsiloxane) (PDMS) and a glass coverslip. The fluid layer lies between the control layer and glass coverslip and contains the microchannels and channel array to trap the bacteria. Media and cells are pumped through the microfluidic channels by on-chip peristaltic pumps and valves that are controlled pneumatically through the top control layer. Each pneumatic valve is controlled by software to apply either vacuum (0.3 bar) or pressure (1.3 bar) to open or close individual valves, respectively. Device fabrication design details are included in Figure S1.

On-device cell culture: Prior to loading cells into the microfluidic device, the fluidic channels were coated with 1% bovine serum albumin (BSA) for 1 h to act as a passivation layer. Then, all the channels were filled with 1 mM IPTG, 0.1% BSA in Luria-Bertani (LB) media (10 g tryptone, 5 g yeast extract, 10 g NaCl per L). A saturated culture of cells (~25 µL) was added through the cell reservoir and pumped into the cell-trapping region. During cell loading, vacuum was applied to the control layer above to open the membrane region. After a sufficient number of cells were pumped underneath the channel array, positive pressure was applied to trap individual cells in those channels. Media was pumped through the microchannels to flush away excess cells. After excess cells were pumped away, media was continuously flowed through the microchannels by gravity flow during the entire experiment.

Time-lapse image acquisition: Steady state cell growth was monitored from 3 to 21 h post inoculation. Fluorescence microscopy was performed on a Nikon Eclipse Ti-E microscope and an Olympus IX83 microscope. The Nikon Eclipse Ti-E microscope was equipped with a 100x Plan Apo lambda, phase contrast, 1.45 N.A., oil immersion objective and a Photometrics Prime95B sCMOS camera with Nikon Elements software (Nikon, Inc.). Fluorescence signals from mCherry and mNeongreen were captured from a Lumencor SpectraX light engine with matched mCherry and YFP filter sets, respectively, from Chroma. The Olympus IX83 microscope was equipped with an Olympus UApo N 100x/1.49 Oil objective and a Hamamatsu EM-CCD Digital Camera operated with MetaMorph Advanced software. Fluorescence signals from mCherry, mNeongreen and BADA were captured from an Olympus U-HGLGPS fluorescence light source with matched TRITC and GFP filters, respectively, from Semrock. Images were captured from at least eight fields of view at a 2 min interval. The channel array was maintained at 37°C with an objective warmer. For all direct comparisons, the same microscope and settings were used.

Data analysis: A period of adaptation following exposure to illumination was observed; thus, data analysis was restricted to periods of steady state. Cell identification and tracking were analyzed by a series of MATLAB programs (The MathWorks, Inc.) (52). The program extracted fluorescence intensity along a line profile down the longitudinal center of each sub-micron channel. The cytoplasmic mCherry line profile showed a flat topped peak on the line where a cell was located, and a local 20% decrease in fluorescence intensity was used to identify cell boundaries after division. Division events were conservatively measured as the time at which one cell became two according to the decrease in fluorescence intensity as described above. Moreover, cell bodies were tracked from frame to frame in order to construct lineages of cell division. The mNeongreen-FtsZ signal was similarly tracked and measured along the length of

the cell. The FtsZ line profile was normalized by cell body intensity in order to minimize intensity differences among frames and different fields of view.

Fluorescent D-amino acid labeling: The fluorescent D-amino acid, BADA, was supplied by VanNieuwenhze and Brun labs. To create BADA, 3-amino-D-alanine was conjugated to BODIPY-FL (53, 54). Stock solutions of BADA (100 mM) were prepared in dimethylsulfoxide (DMSO) as they were poorly soluble in water. The stock solutions were then diluted with LB media to 1 mM BADA with < 2% (vol/vol) DMSO left. To label the cells 3 h post inoculation, the BADA solution (1 mM) was continually pumped through the channel array for 4 min. Excess dye was washed away by pumping LB media through the channel array for 4 min. Fluorescent images were captured at a 2 min interval from at least eight fields of view.

RESULTS

The Min system is required for FtsZ ring disassembly. Quantitative microscopic analysis of cell growth and division on agarose pads is restricted by the limited number of generations that can be observed under batch conditions. To circumvent this problem, a microfluidic-based approach was undertaken to monitor steady-state chemostatic growth of *B. subtilis* over many generations (**Fig S1**). *B. subtilis* divides by septation (or plate formation) in which a division septum is formed first, and remodeling of the septal peptidoglycan occurs as a separate step afterwards that leads to indentation and cell separation (55-57). Thus, cell division events were conservatively defined as a spatial decrease in constitutively-expressed cytoplasmic mCherry fluorescent signal that would indicate cellular indentation (**Fig 1A**). Images were captured every two minutes, and the fluorescence intensity was measured along the length of the microfluidic channel. After inoculation into the microfluidic device, a period of roughly three hours elapsed during which cells appeared to adjust to the growth conditions, and steady-state growth was maintained and monitored over the next 21 hours (**Movie S1**). Microscopic analysis of the rate of septum formation indicated that wild type cells grew with a cell cycle of 39 ± 12 min (**Fig 2A**).

Cell division is mediated by dynamic localization of the division initiation protein, FtsZ (8, 9, 12, 14). FtsZ dynamics were monitored by fluorescence microscopy in a strain encoding an N-terminal fluorescent fusion of mNeongreen introduced at the native site in the chromosome (9). Images were captured every two minutes, and the fluorescence intensity magnitude of FtsZ was measured as a snapshot in the context of a fluorescent mCherry cytoplasmic signal (**Fig 1A**). During steady state growth, FtsZ appeared as a faint uniform cytoplasmic haze with bands of enhanced fluorescence intensity, and a kymograph was generated to track FtsZ dynamics in temporal relation to the cell body (**Fig 3A**, **Fig 1A, Movie S2**). The FtsZ-ring appearance period, defined as the time between the formation of one Z-ring and the formation of another, was found to be similar to that of the cell division period (**Fig 4, Fig S2A**). The Z-ring persistence period, defined as the time between appearance and disappearance of a single

196 focus, was longer than the average period of cell division (**Fig 4, Fig S2B**) likely because FtsZ
197 has been observed to remain transiently at the cell pole after cytokinesis (13, 46, 58).
198 Consistent with previous observations, many cells exhibited a characteristic peak of FtsZ
199 fluorescence intensity near midcell to mediate division, but some cells instead exhibited peak
200 fluorescence at the cell pole after division was complete (**Fig 5A**). We conclude that FtsZ
201 remains polarly localized after cytokinesis.

202 To further explore Z-ring dynamics in the wild type, 100 cells were chosen at random,
203 and a variety of parameters were manually measured. The Z-ring polar duration, defined as the
204 time between septation and the disappearance of the Z-ring (**Fig 4, Fig S2C**) was longer than,
205 and overlapped with, the Z-ring medial delay (**Fig 4, Fig S2D**), defined as the time between
206 septation and the formation of a new Z-ring. Thus, wild type cells transiently experienced
207 multiple FtsZ rings per compartment. Moreover, dissolution of the polar Z-ring coincided with
208 the Z-ring maturation period (**Fig 4, Fig S2E**), defined as the time from first appearance of the
209 Z-ring until maximum Z-ring fluorescence intensity, as FtsZ subunits were redistributed from the
210 pole to the midcell. Finally, the cytokinetic period, defined as the time between Z-ring
211 appearance and cell division was approximately 33 ± 8 min **(Fig 4, Fig S2F)**, which when added
212 to the Z-ring medial delay, ultimately produced a value similar to the cell cycle period (39 ± 12
213 min) (**Fig 4**). We conclude that the dynamic parameters of FtsZ are consistent with a regular
214 cell division cycle despite the transient localization of the Z-ring at the poles.

215 One mechanism that governs FtsZ localization is the Min system (20, 21, 59). To
216 explore the consequences of disruption of the Min system quantitatively, a mutation was
217 introduced in the gene encoding MinD, the membrane localized activator of the FtsZ-inhibitor
218 protein MinC, and the *minD* mutant was monitored during growth in microfluidic channels (**Fig**
219 **1B**). Consistent with a *min* phenotype, the *minD* mutant produced two different cell types: cells
220 that were longer than wild type and very short minicells (**Fig 5B; Movie S3**) (19, 21, 22, 60).
221 Cells mutated for MinD produced multiple FtsZ foci (61) (**Fig 1B; Movie S4**) and kymograph

analysis indicated that the FtsZ-ring persistence period was indefinite such that once formed, the focus did not disappear during the timecourse of observation (**Fig 3B**). Moreover, a greater proportion of *minD* mutant cells exhibited peak FtsZ fluorescence intensity at the poles (**Fig 5C**). We conclude that when a cell divides, the FtsZ focus is split into each daughter cell. In the wild type, the polar FtsZ ring is transient due to antagonism by Min, but in the absence of Min, the ring persists. Our data support models in which the primary function of the Min system during division is to promote FtsZ ring disassembly rather than preventing its formation (23, 46, 62).

The Min system maintains cell size by recycling FtsZ. Mother cells of the *minD* mutant (8.8 ± 3.4 μm, not including minicells) were on average twice as long as the wild type (4.5 ± 1.7 μm) (**Fig 5B**), but the reason *min* mutants were elongated was unclear. One early model suggested that *min* mutants were longer because divisions that produced minicells came at the expense of medial divisions (60, 63). Microscopic analysis, however, indicated that the division time in the *minD* mutant occurred slightly more rapidly than the wild type (**Fig 2A)**. By considering divisions that gave rise to different cell types separately, one quarter of all division events in *minD* gave rise to minicells, and three quarters of division events occurred along the midcell to produce two viable daughters with chromosomes (**Fig 2B**). Thus, midcell divisions occurred at roughly the same average rate as the wild type albeit with a higher standard deviation (**Fig 2B**). The wide variance was due to the occasional longer-than-average division times that gave rise to very long cells which then experienced shorter-than-average division times with multiple division events per compartment that could occur simultaneously or slightly offset from one another (**Fig 6**) (19, 64). We conclude that *min* mutants experience medial division at approximately the same rate as the wild type, and thus, *min* cells are not elongated because polar septation comes at the expense of medial division.

Another factor that could contribute to cell length is the rate of cell elongation, as a faster elongation rate relative to the division rate could give rise to longer cells. By measuring the rate

248 at which the cell poles moved away from one another, the *minD* mutant appeared to elongate
249 more rapidly than the wild type (**Fig 2C**). Elongation, however, occurs by the lateral synthesis of
250 cell wall material distributed along the length of the rod (65-67), and thus, the *minD* mutant
251 might appear to elongate more rapidly simply because longer cells have more positions in
252 between the poles in which to insert new cell wall material per unit time. However, the
253 instantaneous elongation rate, defined as the rate of elongation divided by the length of the cell,
254 was similar for both the wild type and *minD* mutant (**Fig 2D**). Moreover, cells of the wild type
255 and the *minD* mutant accumulated biomass at the same rate as both had indistinguishable
256 growth curves by optical density measurement in broth culture (**Fig 2E**). We conclude the cells
257 of the *minD* mutant elongate at the same rate as the wild type, and thus, the elongation rate
258 cannot explain the presence of elongated cells.

259 Another possible explanation for the increased cell size of *min* mutants is a reduced rate
260 at which FtsZ monomers are added to form FtsZ rings. "Adder" hypotheses for cell growth
261 predict that cell size is dictated by the accumulation of a critical threshold concentration of a
262 particular cell component, in this case, FtsZ (60, 68-70). One requirement for the adder
263 hypothesis is that the rate of FtsZ accumulation must be constant. With respect to FtsZ
264 accumulation, the magnitude of peak FtsZ fluorescence intensity was higher in the wild type
265 than the *minD* mutant (**Fig 5D**), but the *minD* mutant exhibited higher total fluorescence intensity
266 per cell (**Fig 5E**). The higher total fluorescence intensity per cell may be due to the fact that the
267 *minD* cells are longer and maintain multiple Z-rings per compartment. Indeed, when
268 fluorescence intensity was divided by cell length, FtsZ density was found to be nearly identical
269 in both *minD* and the wild type. Thus, the rate of FtsZ synthesis was constant, and FtsZ
270 accumulation was proportional to cell size (**Fig 5F**). We conclude the *minD* mutant cells are
271 elongated because old Z-rings are not recycled, and the cell needs more time and, thus, more
272 biomass to accumulate FtsZ sufficient to form and mature a new Z-ring. We further infer that Z-

ring formation and, subsequently, cell division in *minD* directly depend on the rate of *de novo* FtsZ synthesis.

If FtsZ density accumulated at a rate proportional to cell length (**Fig 5F**), and the *minD* mutant constitutively maintained multiple Z rings, new FtsZ monomers synthesized during growth were likely divided between multiple foci, effectively reducing the rate of local FtsZ accumulation that gives rise to cytokinesis. Indeed, the nascent Z-rings of the *minD* mutant exhibited a 2-3 fold increase in maturation time (**Fig 4, Fig S2E**), likely because the old rings were not dissolved, and each Z-ring independently competed for newly synthesized subunits. We note that the cytokinetic period between FtsZ formation and septation was 2-3 fold longer (**Fig 4, Fig S2F**), suggesting that regeneration of cell division machinery was also delayed. Paradoxically, the cytokinetic period was substantially longer than the cell cycle (**Fig 4**). Each daughter cell of the *minD* mutant, however, was born with at least three persistent Z-rings, one at each pole and one at the future midcell, and additional Z-rings formed at the one-quarter and three-quarter position as the cells grew (**Fig 5C**). Thus, division at the most central Z-ring allowed daughter cells to be born with a preformed medial ring that would eventually drive septation, and as a result the medial Z-ring delay time for *minD* had a negative value (**Fig 4, Fig S2D)**. Despite aberrations in Z-ring parameters, the minD mutant still maintained a similar cell cycle time as the wild type, correlated not with the cytokinetic period but rather with the rate of FtsZ ring appearance (**Fig 4, Fig S2A**). We conclude that the Min system disassembles polar Z-rings to recycle and redistribute monomer units, thereby promoting rapid, singular FtsZ accumulation and maturation at a medial site for the proper maintenance of both the cytokinetic period and cell length (**Fig 4**).

The Min system inhibits peptidoglycan turnover, especially at the cell poles. Mutants defective in the Min system not only produce longer cells but also produce minicells by division at the cell poles. Peptidoglycan at the cell poles is traditionally considered to be “inert” such that

once synthesized, it experiences little *de novo* synthesis and turnover (67, 71-73). To study how minicells formed, cells in the microfluidic device were presented with a sub-generational (4 min) impulse of fluorescent D-amino acids that can be incorporated into peptidoglycan during either synthesis or remodeling (53, 54). In wild type, fluorescent peptidoglycan signal was incorporated along the central part of the cell body with peak fluorescence at the nascent division planes (**Fig 1C**). Moreover, the troughs of peptidoglycan fluorescence intensity coincided with troughs of cytoplasmic fluorescence intensity consistent with the idea that polar peptidoglycan was less dynamic than other positions (**Fig 1C**). Peptidoglycan staining of the *minD* mutant, however, appeared more intense and more uniform than the wild type (**Fig 1D**). In both wild type and the *minD* mutant, peptidoglycan staining was proportional to cell length, but the *minD* mutant accumulated more stain per unit length (**Fig 7A**). Also, unlike the wild type, troughs in cytoplasmic staining intensity in the *minD* mutant did not correspond to decreases in peptidoglycan staining at the cell poles (**Fig 1D**). We conclude that the Min system inhibits peptidoglycan synthesis/remodeling and is an important factor in making the polar peptidoglycan appear “inert”.

We next wanted to determine how the *minD* mutant appeared to accumulate more fluorescent peptidoglycan signal. As above, cells were stained with a 4-min impulse of fluorescent D-amino acids after which, the fluorescent D-amino acids were replaced with unlabeled D-amino acids in the growth medium such that the fluorescence signal would be gradually lost during growth (**Movie S5,S6**). When the amount of fluorescence signal per cell was projected per unit time, *minD* mutant cells with chromosomes experienced a greater overall rate of fluorescence decay than the wild type or *minD* mutant minicells (**Fig 7 B,C, Fig S3 A,B**). Consistent with inert polar peptidoglycan in the wild type, the most intense staining occurred at the nascent division plane, which upon becoming a cell pole remained fluorescent for an extended period of time (**Fig 7D**). The *minD* mutant, however, did not exhibit intense staining at the division plane, and polar staining persisted primarily in minicells (**Fig 7E**). We conclude that

the Min system, at least in *B. subtilis*, appears to restrict peptidoglycan remodeling throughout the cell but has the greatest effect at the cell poles.

Minicells are thought to be physiologically similar to wild type cells due to inheritance of cytoplasmic and membrane proteins, but they lack chromosomes and do not grow. One reason minicells might not grow is that they were thought to be surrounded exclusively by inert polar peptidoglycan, but poles of the *minD* mutant appeared much less inert than the wild type (**Fig 1D**). To further explore the dynamics of polar peptidoglycan observed in the *minD* mutant, the mutant was stained for a longer period of time (20 min). Prolonged exposure of the *minD* mutant to fluorescent D-amino acids resulted in staining of minicell peptidoglycan but only in the most recently formed minicells (**Fig 8**). In each case the entire circumference of the minicell was stained uniformly indicating that old cell pole peptidoglycan was being remodeled at a rate equivalent to the synthesis of the nascent plane (**Fig 8**). Little to no fluorescence was observed in older minicells suggesting that minicells rapidly lost their ability to remodel peptidoglycan (**Fig 8**). We conclude that minicells transiently retain the ability to remodel peptidoglycan, and that the rapid loss of remodeling capacity may be responsible for the inability of minicells to grow. Combined, our microfluidic analysis indicates that the Min system in *B. subtilis* is multifunctional: Min not only disassembles polar FtsZ-rings but also restricts polar peptidoglycan remodeling.

DISCUSSION

Binary fission of rod-shaped bacteria is considered one of the simplest forms of cell division, but it is nonetheless complex. Cells elongate by directing envelope synthesis parallel to the long axis of the cell but must periodically reorient envelope synthesis perpendicular to the long axis to promote cytokinesis. FtsZ forms a ring-like scaffold to recruit the cytokinetic complex for perpendicular peptidoglycan synthesis, and the Min system is thought to help guide FtsZ localization. Here, we quantitatively measure growth and FtsZ dynamics in wild type and a *minD* mutant of *B. subtilis* with a microfluidic device and fluorescence microscopy. We find that the primary function of the Min system is to disassemble FtsZ rings and recycle FtsZ monomers. A failure to recycle FtsZ monomers has a number of consequences on FtsZ dynamics, including the constitutive maintenance of multiple Z-rings per compartment and a longer cytokinetic period. Despite alternations in FtsZ dynamics, however, we find that the *minD* cell cycle is nonetheless much like wild type cell cycle. Moreover, the *min* mutants are so named because they produce small anucleate minicells made exclusively of polar peptidoglycan thought to be relatively inert. Here, we provide evidence that the Min system is responsible for inhibiting polar peptidoglycan turnover and that minicells transiently retain peptidoglycan remodeling capacity.

The function of the Min system is often described as promoting medial Z-ring formation by preventing FtsZ-ring formation at the poles, but our data, along with others, suggest otherwise, at least in *B. subtilis*. Rather than preventing Z-ring assembly, Min is required for FtsZ ring disassembly (23, 30, 35, 46, 62, 74). Evidence that Min does not occlude polar Z-rings comes from spore outgrowth experiments which indicate that FtsZ preferentially localizes to the midcell even when *minD* is mutated, and thus, the *min* phenotype does not manifest in the first generation (75, 76). Instead, FtsZ transiently remains at the cell pole after division and is redistributed to the midcell by the action of Min, such that in the absence of the Min system, FtsZ rings are divided into each new daughter but never dissolve. A Z-ring disassembly model is also consistent with the fact that the Min system co-localizes with nascent septa behind the

371 constricting ring and only encounters FtsZ after septation has completed (77). A disassembly
372 function is also supported by genetic evidence showing that mutants with enhanced Z-ring
373 stability are resistant to the effects of MinCD and mutants with reduced Z-ring stability have
374 enhanced sensitivity (33, 78, 79). That FtsZ may require a specific disassembly factor may also
375 be consistent with the division of *Streptococcus pneumoniae*, which naturally lacks the Min
376 system and produces Z-foci that are not depolymerized. These Z-foci, instead, continually
377 treadmill from the old division site to the new (73).

378 The inability to disassemble Z-rings and recycle FtsZ monomers also explains cell length
379 defects associated with *min* mutants. *min* mutants have long been observed to not only
380 produce minciells but also have mother cells that are longer than the wild type (19, 21, 22, 60).
381 Here, we show that *min* mutants were not elongated due to an extended division time or
382 increased elongation rate but rather due to the dynamics of FtsZ accumulation. In the absence
383 of Min, the persistence of the Z-ring becomes infinite, and cells maintain multiple Z-rings per
384 compartment. Because the density of FtsZ is constant, each Z-ring is forced to compete for
385 newly synthesized FtsZ monomers. Thus, the 2-3 fold increase in cell length was correlated
386 with a 2-3 fold increase in Z-ring maturation time. Our results are consistent with the “adder”
387 hypothesis for growth and cell length control, as *min* mutant cells must become longer to
388 achieve a critical threshold of FtsZ to promote cell division (60, 68-70). Additionally, we
389 observed that the *minD* mutant had a 2-3 fold increase in the cytokinetic period. We conclude
390 that not only was there a failure to recycle FtsZ, but cell division machinery was co-sequestered
391 at latent Z-rings and also required *de novo* synthesis for regeneration (74).

392 Min-mediated disassembly of the latent polar Z-ring coincided with rapid accumulation of
393 a medial Z-ring in the wild type cell cycle. Despite defects in FtsZ dynamics, the *minD* mutant
394 did not suffer a defect in either growth rate or division time, suggesting that the cell cycle was
395 robust and depended on another factor. In the absence of Min, the cytokinetic period exceeded
396 the cell cycle time, Z-ring formation that would give rise to the future division was initiated in the

397 preceding generation. Thus, much like how multifork replication allows daughters to inherit
398 partially replicated chromosomes and grow faster than the replication period, daughter cells
399 inherit a mature Z-ring to complete the cell cycle on time and assemble two new Z-rings for the
400 next generation. Ultimately, the cell cycle of the *min* mutant is governed by the rate of Z-ring
401 appearance, but what governs the Z-ring appearance rate is unclear. One likely regulator of Z-
402 rings is the chromosome because Z-rings are prevented from forming over the mass of the
403 genetic material by nucleoid occlusion (80, 81). We infer that the cell cycle is preserved
404 because the regular period of chromosome replication and segregation dictates the rate at
405 which Z-rings appear, and we note that the Z-ring appearance period is similar to the replication
406 period reported in *B. subtilis* (58, 82, 83).

407 The failure to disassemble Z-rings in the absence of Min leaves behind a preformed
408 polar Z-ring that can give rise to polar cytokinesis and results in the classic phenotype of
409 minicell division. We note, however, that despite the fact that each daughter inherits three Z-
410 rings, two at the pole and one at the midcell, and each Z-ring sequesters division machinery, the
411 division events that gave rise to minicells were nonetheless rare. Competition between the Z-
412 rings for newly synthesized FtsZ monomers and divisome components is unequal, such that the
413 medial Z-ring is stochastically favored. We suspect that medial rings are favored because they
414 are flanked on either side by two chromosomes, each expressing divisome components, and
415 polar Z-rings are disfavored by diffusion being proximal to only one chromosome. Consistent
416 with a positional bias in diffusion-and-capture, medial divisions occur at approximately twice the
417 frequency of minicell divisions, and we found that minicell formation at the new and old pole was
418 equally probable (**Fig 2F**). Regardless on which side of the cell polar-division occurs, the
419 minicell compartment is reduced to a sphere in which half of the peptidoglycan comes from one
420 pole and half comes from the nascent septation event.

421 Polar peptidoglycan of rod-shaped cells has traditionally been considered to be “inert”
422 such that it experiences reduced rates of remodeling relative to the length of the cell. What

423 makes poles behave as though they are inert, however, is unknown. Here, we use a dye that
424 stains peptidoglycan either during synthesis or remodeling to show that in the absence of Min,
425 polar peptidoglycan is indistinguishable from the rest of the cell. How MinD, a protein in the
426 cytoplasm would inhibit peptidoglycan remodeling extracellularly is unclear, but we note the *B.*
427 *subtilis* Min system interacts with a polarly-localized multi-pass transmembrane protein, MinJ
428 (43, 44). MinJ has recently been shown to interact with RodZ, a protein involved in
429 peptidoglycan synthesis/remodeling, and perhaps the MinCDJ complex keeps RodZ away from
430 the poles (84-87). Moreover, why mincells fail to grow is poorly understood, but perhaps, they
431 quickly lose the ability to remodel their peptidoglycan. The loss of remodeling capacity could be
432 due to both the degradation of a single required protein and its corresponding transcript, but we
433 note that the most substantial difference between mother cells and minicells of a *minD* mutant is
434 the absence of the chromosome. Thus, the chromosome may not only direct the cell division
435 cycle, but its presence may either directly or indirectly dictate cell envelope remodeling, and we
436 note that RodZ is a transmembrane protein with a cytoplasmic DNA binding domain (58, 84, 86,
437 88).
438

ACKNOWLEDGEMENTS

We thank Yves Brun and Mike VanNieuwenhze for material support and helpful comments. The work was supported by NIH grant R35 GM131783 to DBK and NIH grant R01 GM113172 to SJ.

442 **Table 1: Strains**

443

Strain	Genotype
DK4393	Δ*hag* Δ*epsE amyE::*$P_{hyspank}$*-mCherry spec*
DK4407	Δ*hag* Δ*epsE amyE::*$P_{hyspank}$*-mCherry spec minD::TnYLB kan*
DK5133	Δ*epsH mNeongreen-ftsZ amyE::*$P_{hyspank}$*-mCherry spec*
DK5155	Δ*epsH mNeongreen-ftsZ amyE::*$P_{hyspank}$*-mCherry spec minD::TnYLB kan*

444

445

REFERENCES

1. **Höltje J-V**. 1998. Growth of the stress-bearing and shape-maintaining murein sacculus of *Escherichia coli*. Microbiol Mol Biol Rev **62**:181-203.
2. **Wang X, Llopis PM, Rudner DZ.** 2013. Organization and segregation of bacterial chromosomes. Nat Rev Genet **14**:191-203.
3. **Errington J, Daniel RA, Scheffers D-J.** 2003. Cytokinesis in bacteria. Microbiol Mol Biol Rev **67**:52-65.
4. **de Boer P, Crossley R, Rothfield L.** 1992. The essential bacterial cell-division protein FtsZ is a GTPase. Nature **359**:254-256.
5. **Erickson HP**. 1995. FtsZ, a prokaryotic homolog of tubulin? Cell **80**:367-370.
6. **Mukherjee A, Lutkenhaus J.** 1994. Guanine nucleotide-dependent assembly of FtsZ into filaments. J Bacteriol **176**:2754-2758.
7. **Mukherjee A, Lutkenhaus J.** 1998. Dynamic assembly of FtsZ regulated by GTP hydrolysis. EMBO J **17**:462-469.
8. **Stricker J, Maddox P, Salmon ED, Erickson HP.** 2002. Rapid assembly dynamics of the *Escherichia coli* FtsZ-ring demonstrated by fluorescence recovery after photobleaching. Proc Natl Acad Sci USA **99**:3171-3175.
9. **Bisson-Filho AW, Hsu Y-P, Squyers GR, Kuru E, Wu F, Jukes C, Sun Y, Dekker C, Holden S, VanNieuwenhze MS, Brun YV, Garner EC.** 2017. Treadmilling by FtsZ filaments drives peptidoglycan synthesis and bacterial cell division. Science **355**:739-743.
10. **Yang X, Lyu X, Miguel A, McQuillen R, Huang KC, Xiao J.** 2017. GTPase activity-coupled treadmilling of the bacterial tubulin FtsZ organizes septal cell wall synthesis. Science **355**:744-747.
11. **Perez AJ, Cesbron Y, Shaw SL, Villicana JB, Tsui H-CT, Boersma MJ, Ye ZA, Tovpeko Y, Dekker C, Holden S, Winkler ME.** 2019. Movement dynamics of divisome proteins and Pbp2x: FtsW in cells of *Streptococcus pneumoniae*. Proc Natl Acad Sci USA **116**:3211-3220.
12. **Bi E, Lutkenhaus J.** 1991. FtsZ ring structure associated with division in *Escherichia coli*. Nature **354**:161-164.
13. **Levin PA, Losick R**. 1996. Transcription factor Spo0A switches the localization of the cell division protein FtsZ from a medial to a bipolar pattern in *Bacillus subtilis*. Genes Dev **10**:478-488.
14. **Ma X, Ehrhardt DW, Margolin W.** 1996. Colocalization of cell division proteins FtsZ and FtsA to cytoskeletal structures in living *Escherichia coli* cells by using green fluorescent protein. Proc Natl Acad Sci USA **93**:12998-13003.
15. **Goehring NW, Gueiros-Filho F, Beckwith J.** 2005. Premature targeting of a cell division protein to midcell allows dissection of divisome assembly in *Escherichia coli*. Gene Dev **19**:127-137.
16. **Weiss DS, Chen JC, Ghigo J-M, Boyd D, Beckwith J.** 1999. Localization of FtsI (PBP3) to the septal ring requires its membrane anchor, the Z ring, FtsA, FtsQ, and FtsL. J Bacteriol **181**:508-520.
17. **Addinall SG, Lutkenhaus J.** 1996. FtsZ-spirals and –arcs determine the shape of the invaginating septa in some mutants of *Escherichia coli*. Mol Microbiol **22**:231-237.
18. **Osawa M, Anderson DE, Erickson HP.** 2008. Reconstitution of contractile FtsZ rings in liposomes. Science **320**:792-794.

19. **Adler HI, Fisher WD, Cohen A, Hardigree AA.** 1967. Miniature *Escherichia coli* cells deficient in DNA. Proc Natl Acad Sci USA **57**:321-326.
20. **Bi E, Lutkenhaus J.** 1993. Cell division inhibitors SulA and MinCD prevent formation of the FtsZ ring. J Bacteriol **175**:1118-1125.
21. **de Boer PAJ, Crossley RE, Rothfield LI.** 1989. A division inhibitor and a topological specificity factor coded for by the minicell locus determine proper placement of the division septum in *E. coli*. Cell **56**:641-649.
22. **Varley AW, Stewart GC.** 1992. The *divIVB* region of the Bacillus subtilis chromosome encodes homologs of *Escherichia coli* septum septum placement (MinCD) and cell shape (MreBCD) determinants. J Bacteriol **174**:6729-6742.
23. **Hu Z, Mukherjee A, Pichoff S, Lutkenhaus J.** 1999. The MinC component of the division site selection system in *Escherichia coli* interacts with FtsZ to prevent polymerization. Proc Natl Acad Sci USA **96**:14819-14824.
24. **Huang J, Cao C, Lutkenhaus J.** 1996. Interaction between FtsZ and inhibitors of cell division. J Bacteriol **178**:5080-5085.
25. **Mulder E, Woldringh CL, Tétart F, Bouché J-P.** 1992. New *minC* mutations suggest different interactions of the same region of division inhibitor MinC with proteins specific for *minD* and *dicB* coinhibition pathways. J Bacteriol 174:35-39.
26. **Hu Z, Lutkenhaus J.** 2003. A conserved sequence at the C-terminus of MinD is required for binding to the membrane and targeting MinC to the septum. Mol Microbiol **47**:345-355.
27. **Szeto TH, Rowland SL, Habrukowich CL, King GF.** 2003. The MinD membrane targeting sequence is a transplantable lipid-binding helix. J Biol Chem **278**:40050-40056.
28. **Hu Z, Saez C, Lutkenhaus J.** 2003. Recruitment of MinC, an inhibitor of Z-ring formation, to the membrane of *Escherichia coli*: role of MinD and MinE. J Bacteriol **185**:196-203.
29. **Lackner LL, Raskin DM, de Boer PAJ**. 2003. ATP-dependent interactions between *Escherichia coli* Min proteins and the phospholipid membrane in vitro. J Bacteriol **185**:735-749.
30. **Park K-T, Dajkovic A, Wissel M, Du S, Lutkenhaus J**. 2018. MinC and FtsZ mutant analysis provides insight into MinC/MinD-mediated Z ring disassembly. J Biol Chem **293**:5834-5846.
31. **Dajkovic A, Lan G, Sun SX, Wirtz D, Lutkenhaus J.** 2008. MinC spatially controls bacterial cytokinesis by antagonizing the scaffolding function of FtsZ. Curr Biol **18**:235-244.
32. **de Boer PAJ, Crossley RE, Rothfield L**. 1992. Roles of MinC and MinD in the site-specific septation block mediated by the MinCDE system of Escherichia coli. J Bacteriol **174**:63-70.
33. **de Oliveira IFF, de Sousa Borges A, Kooij V, Bartosiak-Jentys J, Luirink J, Scheffers D-J.** 2010. Characterization of *ftsZ* mutations that render *Bacillus subtilis* resistant to MinC. PLoS One **5**:e12048.
34. **Shen B, Lutkenhaus J.** 2009. The conserved C-terminal tail of FtsZ is required for the septal localization and division inhibitory activity of $MinC^{C}$/MinD. Mol Microbiol **72**:410-424.
35. **Shen B, Lutkenhaus J.** 2010. Examination of the interaction between FtsZ and $MinC^{N}$ in *E. coli* suggests how MinC disrupts Z rings. Mol Microbiol **75**:1285-1298.

36. **Raskin DM, de Boer PAJ.** 1999. Rapid pole-to-pole oscillation of a protein required for directing division to the middle of *Escherichia coli.* Proc Natl Acad Sci USA **96**:4971-4976.
37. **Hale CA, Meinhardt H, de Boer PAJ.** 2001. Dynamic localization cycle of the cell division regulator MinE in Escherichia coli. EMBO J **20**:1563-1572.
38. **Meinhardt H, de Boer PAJ.** 2001. Pattern formation in *Escherichia coli*: a model for the pole-to-pole oscillations of Min proteins and the localization of the division site. Proc Natl Acad Sci USA **98**:14202-14207.
39. **Hu Z, Lutkenhaus J.** 2001. Topological regulation of cell division in E. coli: spatiotemporal oscillation of MinD requires stimulation of its ATPase by MinE and phospholipid. Mol Cell **7**:1337-1343.
40. **Hu Z, Gogol EP, Lutkenhaus J.** 2002. Dynamic assembly of MinD on phospholipid vesicles regulated by ATP and MinE. Proc. Natl. Acad. Sci USA **99**:6761-6766.
41. **Cha J-H, Stewart GC.** 1997. The *divIVA* minicell locus of *Bacillus subtilis*. J Bacteriol **179**:1671-1683.
42. **Edwards DH, Errington J.** 1997. The *Bacillus subtilis* DivIVA protein targets to the division septum and controls site specificity of cell division. Mol Microbiol **24**:905-915.
43. **Bramkamp M, Emmins R, Weston L, Donovan C, Daniel RA, Errington J**. 2008. A novel component of the division-site selection system of *Bacillus subtilis* and a new mode of action for the division inhibitor MinCD. Mol Microbiol **70**:1556-1569.
44. **Patrick JE, Kearns DB**. 2008. MinJ (YvjD) is a topological determinant of cell division in *Bacillus subtilis*. Mol Microbiol **70**:1166-1179.
45. **Harry EJ, Lewis PJ**. 2003. Early targeting of Min proteins to the cell poles in germinated spores of *Bacillus subtilis*: evidence for division apparatus-independent recruitment of Min proteins to the division site. Mol Microbiol **47**:37-48.
46. **Gregory JA, Becker EC, Pogliano K.** 2008. *Bacillus subtilis* MinC destabilizes FtsZ-rings at new cell poles and contributes to the timing of cell division. Genes Dev **22**:3475-3488.
47. **Balaban NQ, Merrin J, Chait R, Kowalik L, Leibler S.** 2004. Bacterial persistence as a phenotypic switch. Science **305**:1622-1625.
48. **Wang P, Robert L, Pelletier J, Dang WL, Taddei F, Wright A, Jun S.** 2010. Robust growth of Escherichia coli. Curr Biol **20**:1099-1103.
49. **Moffitt JR, Lee JB, Cluzel P.** 2012. The single-cell chemostat: an agarose-based, microfluidic device for high-throughput, single-cell studies of bacteria and bacterial communities. Lab Chip **12**:1487-1494.
50. **Norman TM, Lord ND, Paulsson J, Losick R.** 2013. Memory and modularity in cell-fate decision making. Nature **503**:481-486.
51. **Long Z, Nugent E, Javer A, Cicuta P, Sclavi B, Cosentino Lagomarsino M, Dorfman KD**. 2013. Microfluidic chemostat for measuring single cell dynamics in bacteria. Lab Chip **13**:947-954.
52. **Baker JD, Kysela DT, Zhou J, Madren SM, Wilkens AS, Brun YV, Jacobson SC.** 2016. Programmable, pneumatically actuated microfluidic device with an integrated nanochannel array to track development of individual bacterial. Anal Chem **88**:8476-8483.
53. **Kuru E, Hughes HV, Brown PJ, Hall E, Tekkam S, Cava F, de Pedro MA, Brun YV, Van Nieuwenhze MS.** 2012. In situ probing of newly synthesized peptidoglycan in live bacteria with fluorescent D-amino acids. Angew Chem Int Ed **51**:12519-12523.

54. **Kuru E, Tekkam S, Hall E, Brun YV, Van Nieuwenhze MS.** 2015. Synthesis of fluorescent D-amino acids and their use for probing peptidoglycan synthesis and bacterial growth *in situ*. Nat Protocol **10**:33-52.
55. **Knaysi G**. 1941. Observations on the cell division of some yeasts and bacteria. J Bacteriol **41**:141-153.
56. **Chapman GB, Hillier J.** 1953. Electron microscopy of ultra-thin sections of bacteria: I. Cellular division in *Bacillus cereus*. J Bacteriol **66**:362-373.
57. **Nanninga N, Koppes LJH, de Vries-Tijssen FC**. 1979. The cell cycle of *Bacillus subtilis* as studied by electron microscopy. Arch Microbiol **123**:173-181.
58. **Hajduk IV, Mann R, Rodrigues CDA, Harry EJ.** 2019. The ParB homologs, Spo0J and Noc, together prevent premature midcell Z ring assembly when the early stages of replication are blocked in *Bacillus subtilis*. Mol Microbiol **112**:766-784.
59. **Pichoff S, Lutkenhaus J.** 2001. *Escherichia coli* division inhibitor MinCD blocks septation by preventing Z-ring formation. J Bacteriol **183**:6630-6635.
60. **Teather RM, Collins JF, Donachie WD**. 1974. Quantal behavior of a diffusible factor which initiates septum formation at potential division sites in *Escherichia coli*. J Bacteriol **118**:407-413.
61. **Levin PA, Shim JJ, Grossman AD.** 1998. Effect of *minCD* on FtsZ ring position and polar septation in *Bacillus subtilis*. J Bacteriol **180**:6048-6051.
62. **Johnson JE, Lackner LL, de Boer PAJ.** 2002. Targeting of ^{D}MinC/MinD and ^{D}MinC/DicB complexes to septal rings in *Escherichia coli* suggests a multistep mechanism for MinC-mediated destruction of nascent FtsZ rings. J Bacteriol **184**:2951-2962.
63. **Donachie WD, Begg KJ.** 1996. "Division potential" in Escherichia coli. J Bacteriol **178**:5971-5976.
64. **Åkerlund T, Bernander R, Nordström K.** 1992. Cell division in Escherichia coli minB mutants. Mol Microbiol **6**:2073-2083.
65. **Mauck J, Chan L, Glaser L, Williamson J.** 1972. Mode of cell wall growth of *Bacillus megaterium*. J Bacteriol **109**:373-378.
66. **Burman LG, Raichler J, Park JT.** 1983. Evidence of diffuse growth of the cylindrical portion of the Escherichia coli murein sacculus. J Bacteriol **155**:983-988.
67. **Tiyanont K, Doan T, Lazarus MB, Fang X, Rudner DZ, Walker S.** 2006. Imaging peptidoglycan biosynthesis in *Bacillus subtilis* with fluorescent antibiotics. Proc. Natl. Acad. Sci. USA **103**:11033-11038.
68. **Jaffé A, Boye E, D'ari R.** 1990. Rule governing the division pattern in *Escherichia coli minB* and wild-type filaments. J Bacteriol 172:3500-3502.
69. **Campos M, Surovtsev IV, Kato S, Paintdakhi A, Beltran B, Ebmeier SE, Jacobs-Wagner C.** 2014. A constant size extension drives bacterial cell size homeostasis. Cell **159**:1433-1446.
70. **Si F, Le Treut G, Sauls JT, Vadia S, Levin PA, Jun S.** 2019. Mechanistic origin of cell-size control and homeostasis in bacteria. Curr Biol **29**:1760-1770.
71. **de Pedro MA, Donachie WD, Holtje J-V, Schwarz H.** 2001. Constitutive septal murein synthesis in *Escherichia coli* with impaired activity of the morphogenetic proteins RodA and penicillin-binding protein 2. J Bacteriol **183**:4115-4126.
72. **Mobley HLT, Koch AL, Doyle RJ, Streips UN.** 1984. Insertion and fate of the cell wall in Bacillus subtilis. J Bacteriol **158**:169-179.

73. **Boersma MJ, Kuru E, Rittichier JT, Van Nieuwenhze MS, Brun YV, Winkler ME.** 2015. Minimal peptidoglycan (PG) turnover in wild-type and PG hydrolase and cell division mutants of *Streptococcus pneumoniae* D39 growing planktonically and in host-relevant biofilms. J Bacteriol **197**:3472-3485.
74. **Van Baarle S, Bramkamp M.** 2010. The MinCDJ system in *Bacillus subtilis* prevents minicell formation by promoting divisome disassembly. PLoS One **5**:e9850.
75. **Migocki MD, Freeman MK, Wake G, Harry EJ.** 2002. The Min system is not required for precise placement of the midcell Z ring in *Bacillus subitlis*. EMBO rep **3**:1163-1167.
76. **Rodrigues CDA, Harry EJ.** 2012. The Min system and nucleoid occlusion are not required for identifying the division site in *Bacillus subtilis* but ensure its efficient utilization. PLoS Genet **8**:e1002561.
77. **Eswaramoorthy P, Erb ML, Gregory JA, Silverman J, Pogliano K, Pogliano J, Ramamurthi KS.** 2011. Cellular architecture mediates DivIVA ultrastructure and regulates Min activity in *Bacillus subtilis*. mBio **2**:e00257-11.
78. **Levin PA, Schwartz RL, Grossman AD**. 2001. Polymer stability plays an important role in the positional regulation of FtsZ. J Bacteriol **183**:5449-5452.
79. **Yu X-C, Margolin W**. 2000. Deletion of the *min* operon results in increased thermosensitivity of an *ftsZ84* mutant and abnormal FtsZ ring assembly, placement, and disassembly. J Bacteriol **182**:6203-6213.
80. **Mulder E, Woldringh CL.** 1989. Actively replicating nucleoids influence positioning of division sites in *Escherichia coli* filaments forming cells lacking DNA. J Bacteriol **171**:4303-4314.
81. **Woldringh CL, Mulder E, Huls PG, Vischer N.** 1991. Toporegulation of bacterial division according to the nucleoid occlusion model. Res Microbiol **142**:309-320.
82. **Sharpe ME, Hauser PM, Sharpe RG, Errington J.** 1998. *Bacillus subtilis* cell cycle as studied by fluorescence microscopy: constancy of cell length at initiation of DNA replication and evidence for active nucleoid partitioning. J Bacteriol **180**:547-555.
83. **Moriya S, Rashid RA, Andrade Rodrigues CD, Harry EJ.** 2010. Influence of the nucleoid and the early stages of DNA replication on positioning the division site in *Bacillus subtilis*. Mol Microbiol **76**:634-647.
84. **Shiomi D, Sakai M, Niki H**. 2008. Determination of bacterial rod shape by a novel cytoskeletal membrane protein. EMBO J **27**:3081-3091.
85. **Bendezú FO, Hale CA, Bernhardt TG, de Boer PAJ.** 2009. RodZ (YpfA) is required for proper assembly of the MreB actin cytoskeleton and cell shape in *E. coli*. EMBO J **28**:193-204.
86. **Alyahya SA, Alexander R, Costa T, Henriques AO, Emonet T, Jacobs-Wagner C.** 2009. RodZ, a component of the bacterial core morphogenetic apparatus. Proc Natl Acad Sci USA **106**:1239-1244.
87. **Muchová K, Chromiková Z, Valenčiková R, Barák I**. 2018. Interaction of the morphogenetic protein RodZ with the *Bacillus subtilis* Min system. Front Microbiol **8**:2650.
88. **Adams DW, Wu LJ, Errington J.** 2015. Nucleoid occlusion protein Noc recruits DNA to the bacterial cell membrane. EMBO J **34**:491-501.

679 **FIGURE LEGENDS**

680 **Figure 1: Microfluidic analysis of growth and division in wild type and *min* mutants.**
681 Snapshot fluorescent microscopy of a microfluidic channel for wild type (A,C) and a *minD*
682 mutant (B,D) growing at steady state. A and B) Fluorescence microscopy of cells in a
683 microfluidic channel expressing cytoplasmic mCherry protein false colored red (top),
684 mNeongreen-FtsZ false colored green (middle), and an overlay of the two colors (bottom).
685 Graphs are a quantitative analysis of mCherry fluorescence intensity (red line) and mNeongreen
686 fluorescence intensity (green line) to match the fluorescence microscopy images immediately
687 above. All images are reproduced at the same magnification. C and D) Fluorescence
688 microscopy of a microfluidic channel for wild type (A,C) and a *minD* mutant (B,D) growing at
689 steady state. Cytoplasmic mCherry protein false colored red (top), and peptidoglycan stained
690 with BADA false colored green (bottom). Graphs are a quantitative analysis of mCherry
691 fluorescence intensity (red) and BADA fluorescence intensity (green) to match the fluorescence
692 microscopy images immediately above. All images are reproduced at the same magnification.
693 Wild type (DK5133) and a *minD* mutant (DK5155) were used to generate all of the data in this
694 figure.

695

696 **Figure 2: Cells mutated for the *min* system divide faster than wild type.** A) A histogram of
697 the division time of individual cells of wild type (gray) and a *minD* mutant (blue) measured by
698 microscopic analysis. Division events were defined by a local 20% decrease in mCherry
699 (cytoplasmic) fluorescence intensity below a threshold value. More than 3000 division events
700 were counted per dataset. Minicells were excluded from the division time analysis as once they
701 are formed, minicells never divide. B) A histogram of division time of individual cells of the
702 *minD* mutant using the dataset in panel A to separately determine the time elapsed between
703 medial and minicell divisions. The time between medial division events (cyan) was determined
704 as those events that gave rise to two separate cells with chromosomes. The time between

minicell divisions (magenta) was determined to be the time between the formation of a cell pole and the formation of a division plane at that pole to give rise to a minicell. C) Cell elongation rates were measured as the rate at which the cell poles moved apart from one another in wild type (gray) and a *minD* mutant (blue). The growth of over 2500 cells was measured for each strain. Minicells were excluded from the elongation rate analysis as once they formed, minicells do not elongate. D) Data from panel 2C was replotted as the instantaneous increase in cell length per total length of the cell observed. E) Growth curve of wild type (gray) and a minD mutant (blue) growing in highly agitated LB broth at 37°C and optical density was measured with a spectrophotometer at 600 nm wavelength. Wild type (DK5133) and a *minD* mutant (DK5155) were used to generate all of the data in this figure. F) Frequency histogram of division time that gives rise to minicells at either the old cell pole (yellow) or the new cell pole (violet). Old cell poles were defined by the pole that last experienced a polar division event. New cell poles were defined by the pole that had not previously experienced a polar division event.

Figure 3. FtsZ foci remain at the poles indefinitely in the absence of Min. Kymograph analysis of wild type (A) and a *minD* mutant (B) of cytoplasmic mCherry signal false colored red (top) and mNeongreen-FtsZ intensity false colored green (middle), and an overlay of the red and green channels (bottom). In each panel a single microfluidic channel was followed in a series of stacked snapshots taken at 2 minute intervals to assemble the kymograph. All images reproduced at the same magnification. Wild type (DK5133) and a *minD* mutant (DK5155) were used to generate all of the data in this figure.

Figure 4: The cytokinetic period is longer than a cell cycle in a *minD* mutant. Top) Sample kymograph analysis of a wild type (A) and a *minD* mutant (B) microfluidic channel in which cytoplasmic mCherry signal is false colored red (left) and overlayed with mNeongreen-FtsZ that is false colored green (right). Events necessary for defining division paramaters are

731 indicated and labeled a, septation; b, detection of a nascent Z-ring; c, disappearance of a Z-ring;
732 d, FtsZ peak intensity achieved. Thin white lines are include to indicate cell tracking and lineage
733 analysis. Middle) Graphs of 100 manually tracked wild type (gray) and minD (blue) cell cycles
734 presented as bars of average values and whiskers of standard deviation for the following
735 parameters: “Cell cycle” is the time between septation events (between consecutive “a” events);
736 Z-ring appearance period is the time between the formation of one Z-ring and another (between
737 consecutive “b” events); “Z-ring persistence period” is the time between the formation of a Z-ring
738 and the disappearance of that Z-ring (between consecutive “b” and “c” events); “Z-ring polar
739 duration” is the time between a septation event and the disappearance of the Z-ring resulting
740 from that septation events (between consecutive “a” and “c” events); “Z-ring medial delay” is the
741 time between a septation event and the formation of a Z-ring that will eventually give rise to the
742 next medial division event (between an “a” event and a “b” event that will give rise to the next
743 round of septation); “Z-ring maturation period” is the time between Z-ring formation and when
744 that Z-ring achieves peak local intensity (between consecutive “a” and “d” events); and the
745 “cytokinetic period” is the time between Z-ring formation and septation directed by that Z-ring
746 (between a “b” event and the “a” event that is caused by that particular Z-ring). The raw data
747 histograms for each bar are presented in Fig S2. Bottom) Timeline representations of the
748 various events indicated in the bar graph depicted in cartoon form, color coded to match the
749 indicated parameter of like color above, and annotated with relevant events marked by the
750 defining letters.
751
752 **Figure 5: FtsZ density is constant in both the wild type and the *minD* mutant.** A) A
753 frequency histogram of the location of snapshot peak FtsZ intensity plotted relative to total cell
754 length for wild type. The poles of the cell have relative position values of 0 and 1.0 whereas the
755 midcell has a value of 0.5. B) A frequency histogram of cell length distribution of wild type
756 (gray) and a *minD* mutant (blue). The *minD* mutant has two peaks, a shorter peak

757 corresponding to “minicells” and a longer peak corresponding to “mother” cells that have
758 chromosomes and are capable of division. C) A frequency histogram of the location of
759 snapshot peak FtsZ intensity plotted relative to total cell length for *minD*. D) A frequency
760 histogram of peak FtsZ fluorescence intensity per cell. For each frame, a line scan through the
761 longitudinal axis of the cell determined the location of peak fluorescence intensity and peak
762 fluorescence magnitude was recorded. Wild type distribution (gray); *minD* distribution (blue).
763 E) A frequency histogram of total FtsZ fluorescence intensity per cell was measured by
764 integrating the area under the line scans from panel D. F) A frequency histogram of total
765 fluorescence intensity was divided by cell length for each individual. Measurements were taken
766 for 9000 cells of growing wild type (DK5133) amounting to over 30,000 measurements, and
767 3000 cells of growing minD (DK5155) for over 20,000 measurements to generate the data in
768 this figure.
769
770 **Figure 6. Some cells of a *minD* mutant experience multiple simultaneous division.**
771 Kymograph analysis of cytoplasmic mCherry fluorescence intensity of single channels of a wild
772 type (left) or *minD* (middle and right) mutant. Wild type cells experience regular division once
773 per cell cycle (caret, left panel) but occasionally multiple simultaneous (carets middle panel) or
774 slightly offset (carets right panel) division events were observed in the *minD* mutant. The
775 presented kymographs of individual wells were representative of general trends taken from the
776 image stacks generated in Figure 1. Wild type (DK5133) and a *minD* mutant (DK5155) were
777 used to generate all of the data in this figure.
778
779 **Figure 7. *minD* mutants lose BADA staining fluorescence intensity faster than the wild**
780 **type.** Cells were grown in the presence of the peptidoglycan synthesis/remodeling indicator
781 stain BADA for 4 minutes, the stain was washed out of the microfluidic device for 8 minutes and
782 then fluorescence intensity was tracked in time. A) A graph of the total BADA intensity per cell

per the length of the cell measured in the first frame of the experiment. Each dot represents an individual cell of wild type (gray) and *minD* mutant (blue). B) A graph of the total BADA intensity per cell per unit time after washout of fluorescent D-amino acids. Gray, wild type; Blue; *minD* mutant, Cyan, mother cells of the *minD* mutant with chromosomes, and magenta, minicells of the *minD* mutant. C) A graph of the rate of decrease in BADA intensity loss as measured by the slope of the lines in Figure 7B. D) A representative kymograph of wild type after BADA washout. E) A representative kymograph of *minD* after BADA washout. The wild type (DK4393) and *minD* mutant (DK4407) strains were used for all panels in this figure. Over 500 measurements were taken for each strain.

Figure 8. Recently formed minicells are proficient for remodeling of the polar peptidoglycan. A) Microfluidic analysis of a *minD* (DK4407) mutant expressing cytoplasmic mCherry false colored red (left) and stained for 20 minutes with the fluorescent D-amino acid BADA false colored green (right). Individual areas of the channels are highlighted by white boxes and numbered. Below are enlarged images of the boxes with the corresponding number to increase detail.

Figure S1. Diagram of the microfluidic device. Black lines indicate microfluidic channels. Open circles indicate media/reagent input/output reservoirs. Closed circles indicate the location of peristaltic valves. Three valves in parallel indicate a peristaltic pump. Location of the nanochannel array imaged by fluorescence microscopy indicated by a red box. The same device was used previously in (Baker et al., 2016).

Figure S2. Data histograms of FtsZ parameters used to generate Figure 4. 100 cells were manually tracked and measured through a cell cycle to generate the data for each panel. Data are presented as gray bars for wild type (DK5133) and as blue bars for the *minD* mutant

(DK5155). A) Frequency histogram of the Z-ring appearance period defined as the time between the formation of one Z-ring and the next Z-ring. B) Frequency histogram of the Z-ring persistence period defined by the time between the formation of a Z-ring and the disappearance of that Z-ring. Note, no data are provided for the *minD* mutant as the Z-rings of a *minD* mutant did not disappear and the persistence period was effectively infinite. C) Frequency histogram of the Z-ring polar duration defined as the time between a septation event and the disappearance of the Z-ring resulting from that septation events. Note, no data are provided for the *minD* mutant as the Z-rings of a *minD* mutant did not disappear and the polar duration period was effectively infinite. D) Frequency histogram of the Z-ring medial delay defined as the time between a septation event and the formation of a Z-ring that will eventually give rise to the next medial division event. Note that the Z-ring medial delay of the *minD* mutant was often negative because the medial Z-ring that would eventually promote cell division was formed in the preceding generation. E) Frequency histogram of the Z-ring maturation period defined as the time between Z-ring formation and when that Z-ring achieves peak local intensity. F) Frequency histogram of the cytokinetic period defined as the time between Z-ring formation and septation directed by that Z-ring.

Figure S3. The *minD* mutant accumulates and loses fluorescent BADA signal more rapidly than the wild type. A) Total BADA fluorescence intensity after a 4-min staining impulse and washout of the BADA stain in the wild type (DK4393). Points are the average, and whiskers are the standard deviation of over 500 measurements. B) Total BADA fluorescence intensity after a 4-minute staining impulse and washout of the BADA stain in the *minD* mutant (DK4407). Points are the average, and whiskers are the standard deviation of over 500 measurements. Cyan indicates measurements of the long mother cells with nucleoids, and magenta indicates measurements of minicells.

Figure S4. A minicell redistributed peptidoglycan stain from its old cell pole to its new cell pole. Cells were stained with BADA for 4 min, then media lacking BADA was introduced to wash out the dye, and a kymograph of one channel was generated. Here, we highlight an instance in which a minicell was formed by polar division soon after the dye had been removed such that old pole was stained but the division plane and resulting new pole was not (white caret). Over time, the fluorescent signal incorporated into the peptidoglycan becomes uniformly redistributed around the circumference of the minicell (black caret).

Movie S1: Wild type growth in microfluidic channels. Constitutive cytoplasmic mCherry, false colored red. Strain DK5133. Movies are 200 frames over 400 min at a rate of 1 frame/2 min.

Movie S2: Wild type growth in microfluidic channels with fluorescent FtsZ. Constitutive cytoplasmic mCherry, false colored red, and a mNeongreen-FtsZ, false colored green. Strain DK5133. Movies are 200 frames over 400 min at a rate of 1 frame/2 min.

Movie S3: *minD* mutant growth in microfluidic channels. Constitutive cytoplasmic mCherry, false colored red. Strain DK5155. Movies are 200 frames over 400 min at a rate of 1 frame/2 min.

Movie S4: *minD* mutant growth in microfluidic channels with fluorescent FtsZ. Constitutive cytoplasmic mCherry, false colored red, and a mNeongreen-FtsZ, false colored green. Strain DK5155. Movies are 200 frames over 400 min at a rate of 1 frame/2 min.

Movie S5: Wild type growth in microfluidic channels with fluorescent BADA that stains newly synthesized/remodeled peptidoglycan. Constitutive cytoplasmic mCherry, false colored red, and stained with a 4 minute pulse of BADA, false colored green. Strain DK4393. BADA was washed out of the channel for 4 minutes after which, imaging was recommenced. Movies are 60 frames over 120 min at a rate of 1 frame/2 min.

Movie S6: *minD* growth in microfluidic channels with fluorescent BADA that stains newly synthesized/remodeled peptidoglycan. Constitutive cytoplasmic mCherry, false colored red, and stained with a 4 minute pulse of BADA, false colored green. Strain DK4407. BADA was washed out of the channel for 4 minutes after which, imaging was recommenced. Movies are 60 frames over 120 min at a rate of 1 frame/2 min.

Figure 1

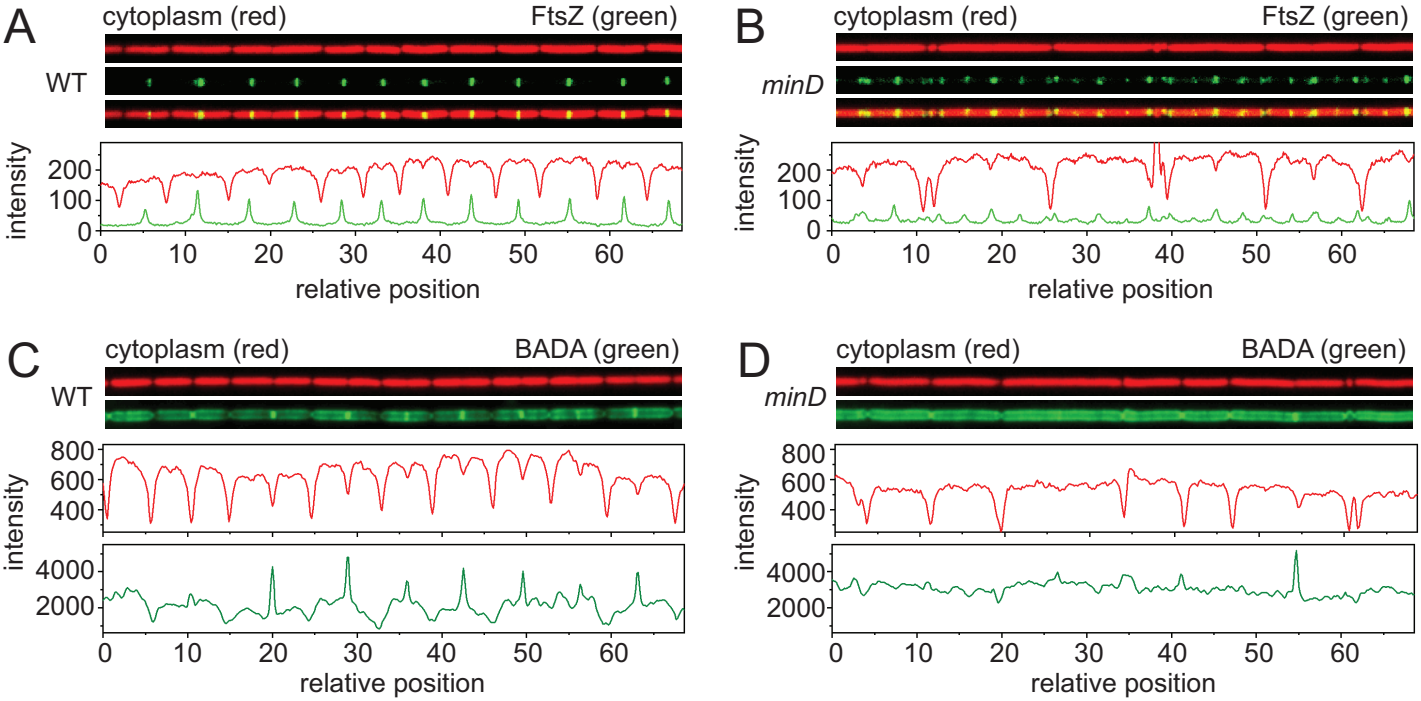
A
cytoplasm (red)
FtsZ (green)
WT
intensity
200
100
0
0
10
20
30
40
50
60
relative position
B
cytoplasm (red)
FtsZ (green)
minD
intensity
200
100
0
0
10
20
30
40
50
60
relative position
C
cytoplasm (red)
BADA (green)
WT
intensity
800
600
400
4000
2000
0
10
20
30
40
50
60
relative position
D
cytoplasm (red)
BADA (green)
minD
intensity
800
600
400
4000
2000
0
10
20
30
40
50
60
relative position

Figure 2

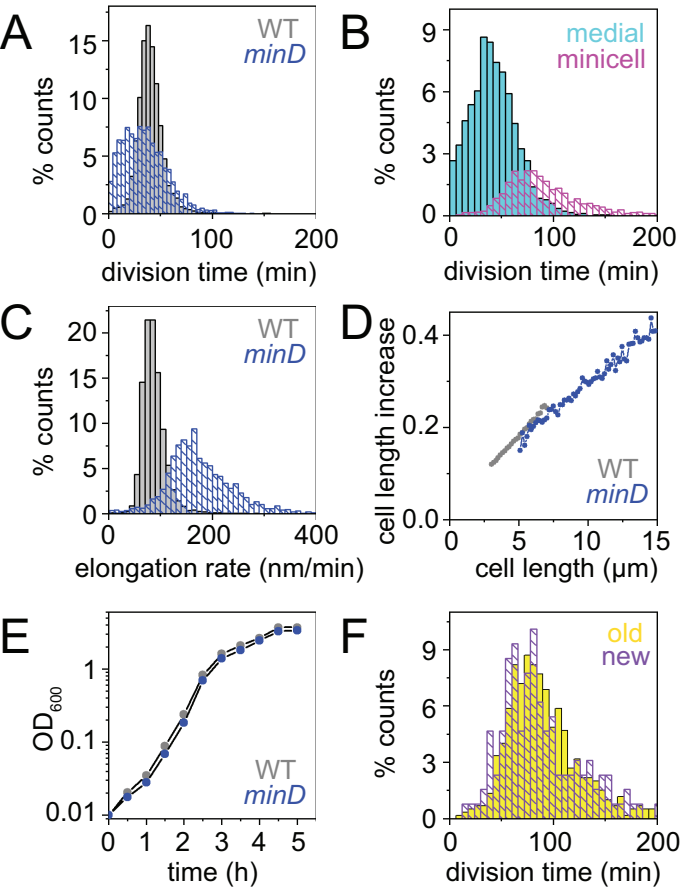
A
WT
minD
% counts
division time (min)
B
medial
minicell
% counts
division time (min)
C
WT
minD
% counts
elongation rate (nm/min)
D
cell length increase
cell length (μm)
WT
minD
E
OD600
WT
minD
time (h)
F
old
new
% counts
division time (min)

Figure 3

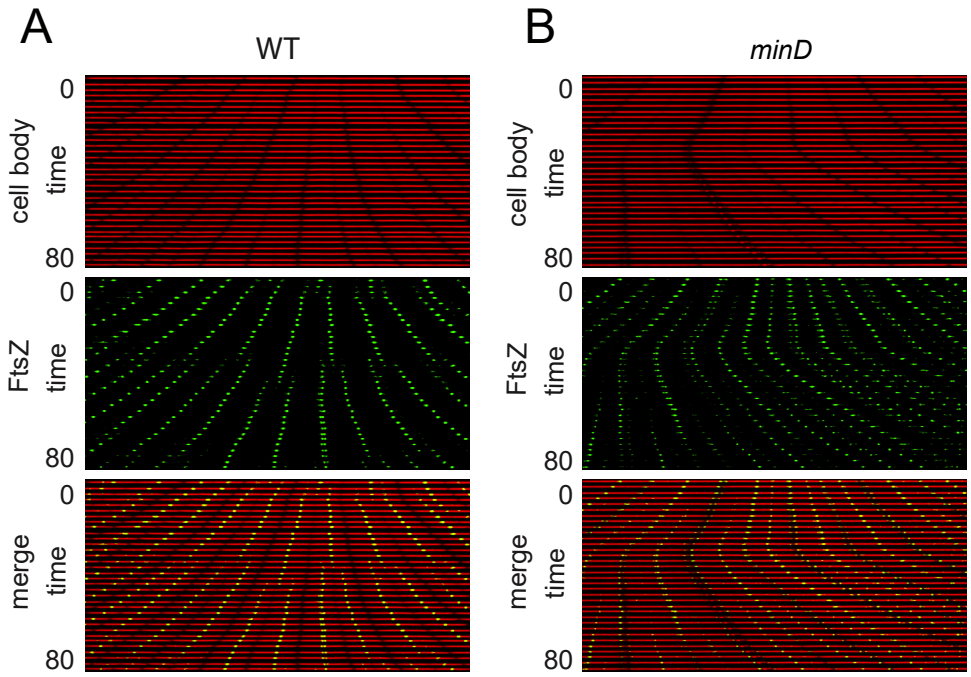

Figure 4

Kymograph event key

a. septation
b. FtsZ ring appears
c. FtsZ ring disappears
d. FtsZ ring peak intensity

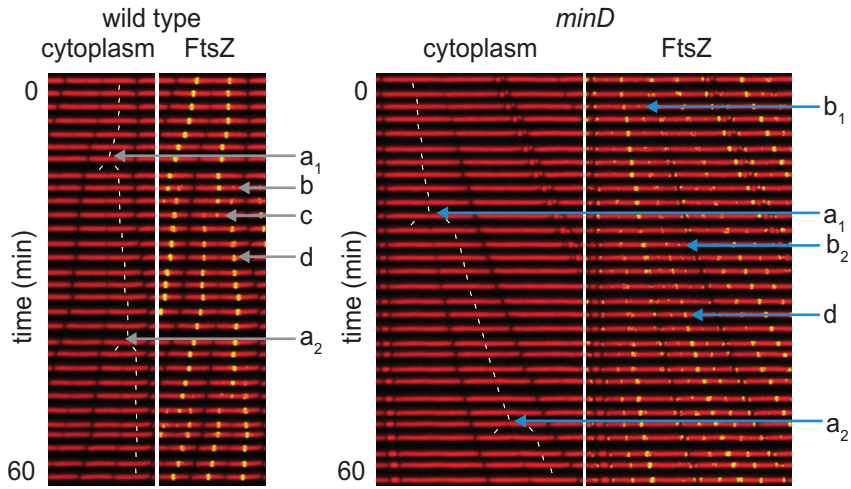

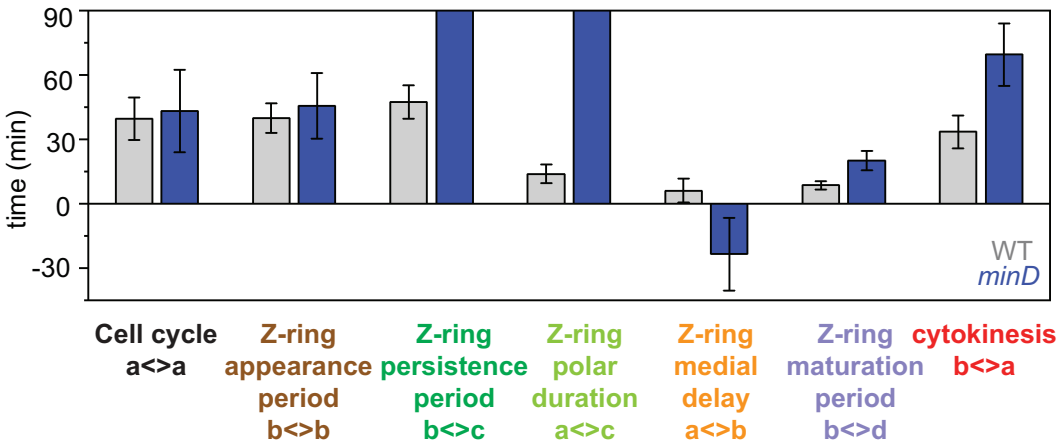

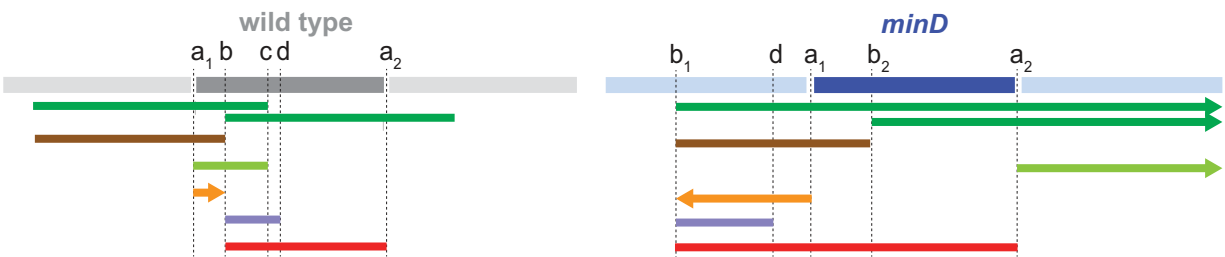

Figure 5

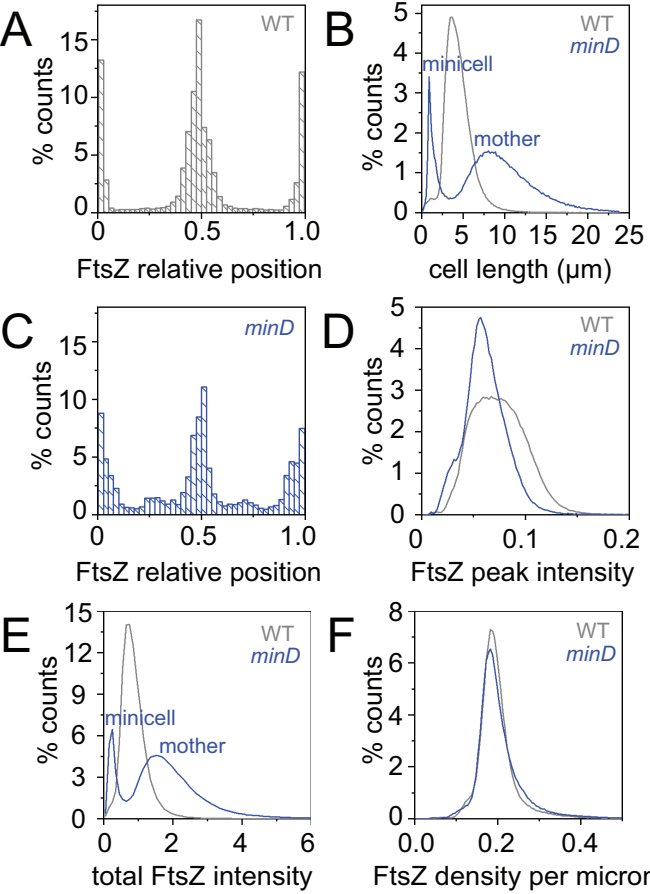
A
WT
% counts
FtsZ relative position
B
WT
minD
minicell
mother
% counts
cell length (μm)
C
minD
% counts
FtsZ relative position
D
WT
minD
% counts
FtsZ peak intensity
E
WT
minD
minicell
mother
% counts
total FtsZ intensity
F
WT
minD
% counts
FtsZ density per micron

Figure 6

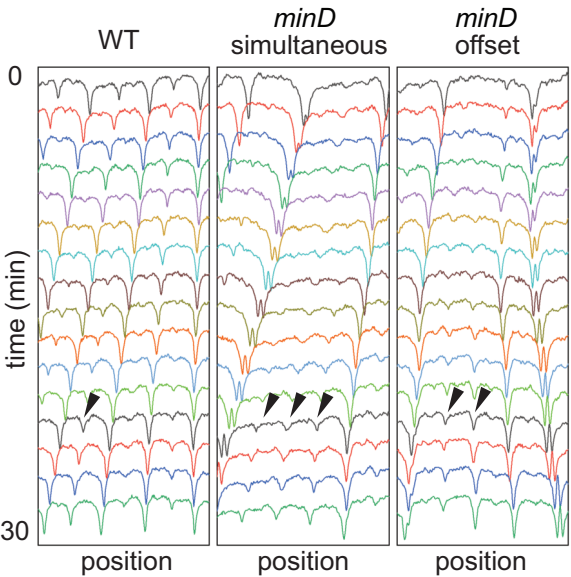
WT
minD
simultaneous
minD
offset
0
time (min)
30
position
position
position

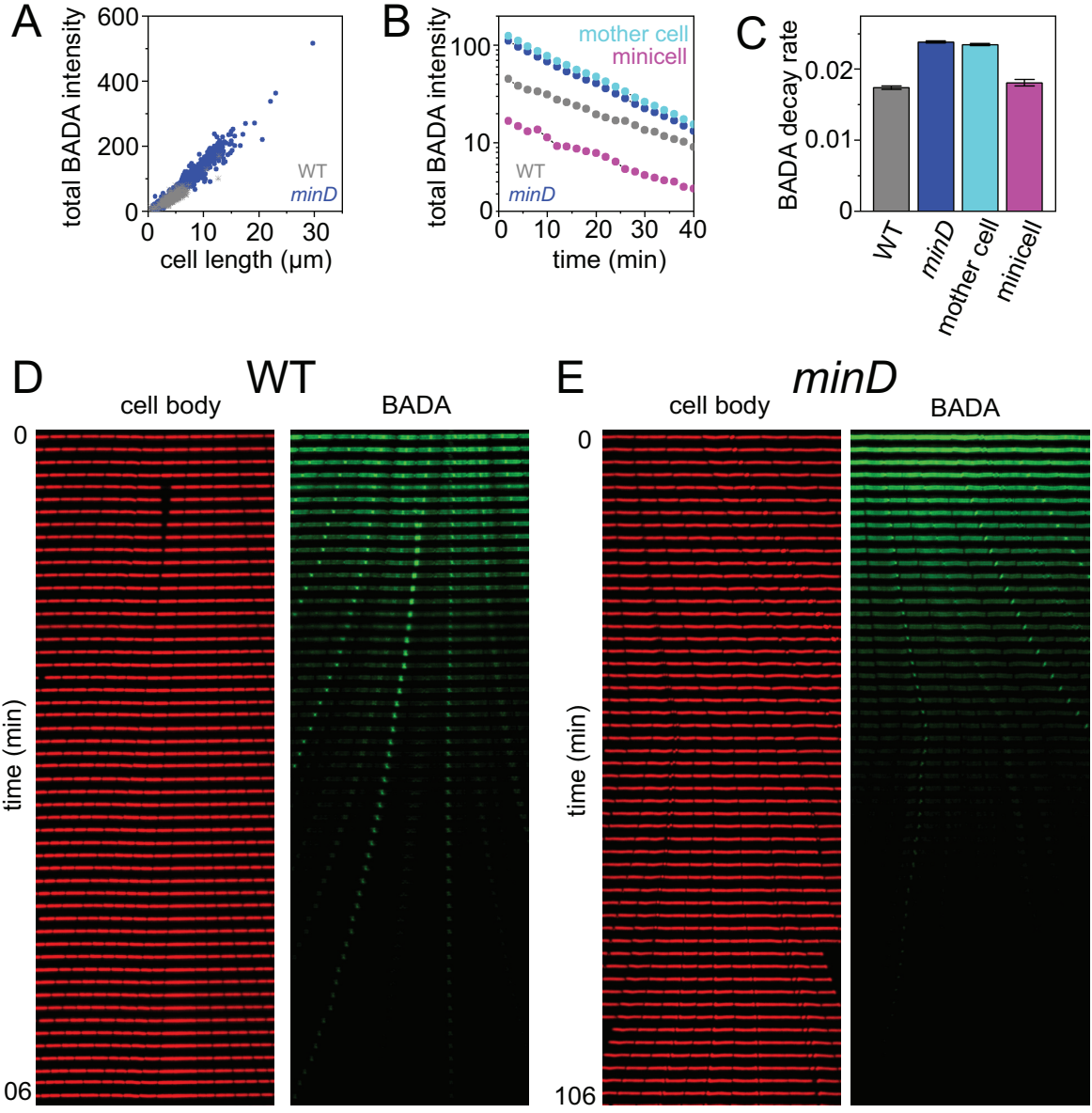
A
total BADA intensity
600
400
200
0
0
10
20
30
cell length (μm)
WT
minD
B
total BADA intensity
100
10
0
0
10
20
30
40
time (min)
mother cell
minicell
WT
minD
C
BADA decay rate
0.02
0.01
0
WT
minD
mother cell
minicell
D
WT
cell body
BADA
0
time (min)
106
E
minD
cell body
BADA
0
time (min)
106

Figure 8

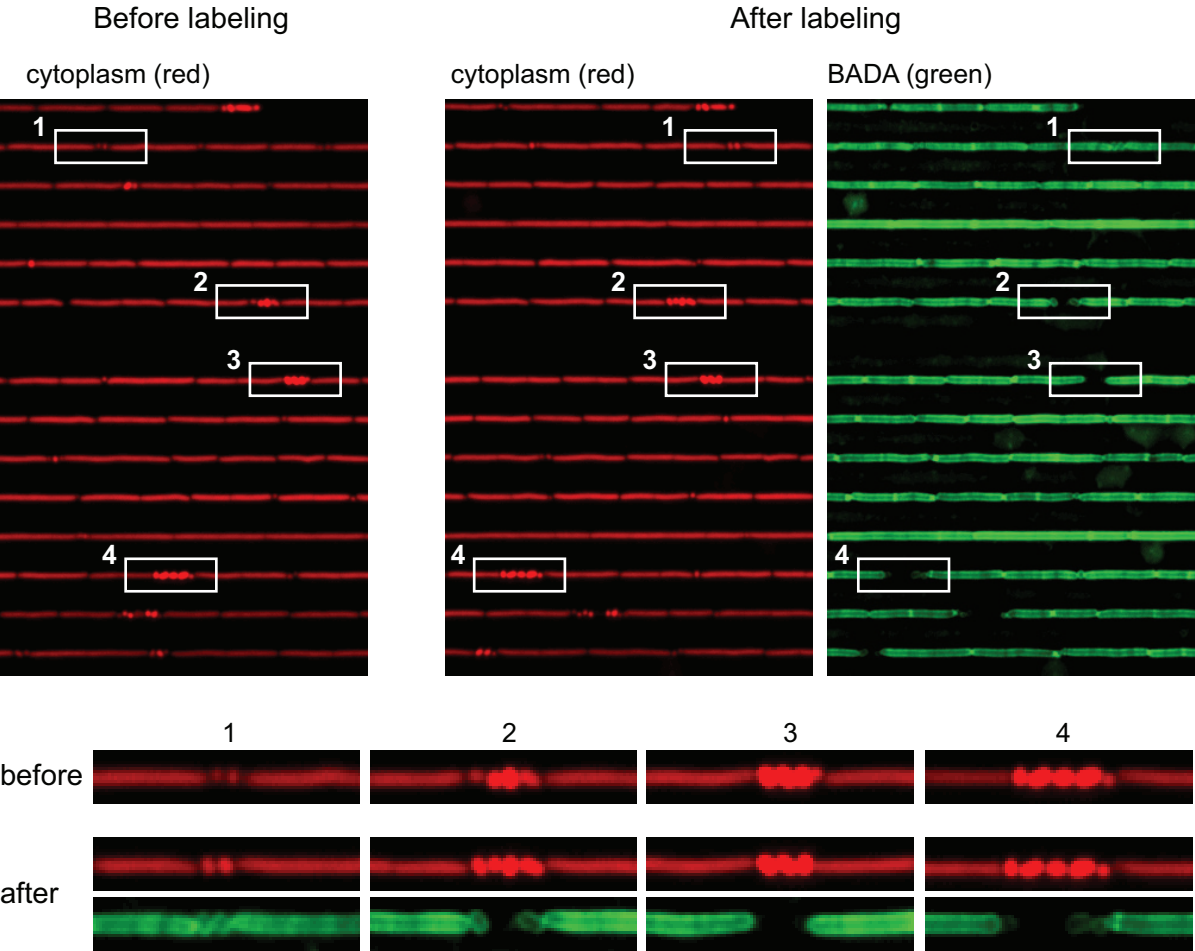
Before labeling
After labeling
cytoplasm (red)
cytoplasm (red)
BADA (green)
1
2
3
4
1
2
3
4
1
2
3
4
1
2
3
4
before
after